Lasers in Manufacturing Conference 2019

Laser-induced Periodic Surface Structures (LIPSS) on stainless steel moulds for thermoplastic composite materials manufacturing

M. Feinaeugle[a*], M. Mezera[a], G.R.B.E. Römer[a]

[a]*Chair of Laser Processing, Department of Mechanics of Solids, Surfaces and Systems (MS3), Faculty of Engineering Technology, University of Twente, Enschede, 7522NB, The Netherlands*

Abstract

Steel moulds are widely used as forming tools during the fabrication of fibre reinforced thermoplastic composite parts. The aim of this work is to study sub-micron laser-induced surface modifications which help to control interfacial properties, such as undesirable sticking, between the composite polymer and the steel mould material. Stainless steel (AISI 430) samples were machined with a laser with wavelength of λ = 515 nm and 7 ps pulse duration. The periodicity of the Laser-induced Periodic Surface Structures (LIPSS) was determined, via fast Fourier transform of scanning electron microscope images, as a function of input parameters, such as effective number of laser pulses, pulse energy and accumulated fluence. Above a certain threshold, LIPSS appear over a broad range of fluences. Spatial frequencies were found to be between about λ/10 and ~λ for laser pulse energies of up to ~1 µJ. First results from experiments on interaction of composite polymers and steel moulds are also shown.

Keywords: micro processing; surface functionalisation; laser-induced periodic surface structure; stainless steel; thermoplastic composites;

1. Introduction

During the fabrication of thermoplastic composites, moulds are applied for forming of parts. Thereby, stainless steel is widely used as a base material for these moulds due to the wealth and ease of applying

* Corresponding author. Tel.: +31-53-4894548.
E-mail address: m.feinaeugle@utwente.nl

methods for mould fabrication. However, under certain conditions, the prepared composite parts will experience partial or complete sticking to the mould, which leads to build-up of polymer material, and as a result reduces throughput and lifetime of the mould (Packham, 2002). Further accumulation of polymer will then occur during subsequent forming process steps which lead to increased sticking or contamination from loose polymer particles. To prevent polymer-metal adhesion, intermediate films are currently used, such as solid polyimide ('Kapton') or spray-on hydrocarbon-based release agents (Critchlow et al., 2006). In order to reduce these single-use, costly, potentially contaminating and hazardous films, a more permanent modification to the moulds is desired. Therefore the aim of the this work is to modify the surface geometry of the mould material to reduce adhesion between the polymers from the thermoplastic composites and the metallic moulds. Here, a laser-based process is investigated to create such modifications on the nanoscale.

The effects of repeated irradiation of a laser on a material surface have been studied not late after the advent of the laser and very early, structures on the order of magnitude of the incident laser wavelength have been discovered by Birnbaum on semiconductors (Birnbaum, 1965). The repeated structures were termed laser-induced periodic surface structures (LIPSS) also referred to as periodic surface features (Bonse et al., 2017) and patterns (Temple and Soileau, 1981), nanostructures (Römer et al., 2009), ripples (Fauchet and Siegman, 1982) or nanogratings (Birnbaum, 1965) and can appear on a broad range of materials, including metals, polymers or dielectrics (Baudach et al., 1999; Csete et al., 2004; Jee et al., 1988; Siegrist et al., 1973; Temple and Soileau, 1981; Young et al., 1983). Their geometrical properties (periodicity, amplitude and regularity) depend on the incident laser parameters and material properties (Bonse et al., 2017; Römer et al., 2014).

In this study, we investigate the emergence of LIPSS on mirror-polished AISI430 stainless steel, a typical mould material for the consolidation process during thermoplastic composite production. In the following, the experimental approach is introduced and results from parametric studies of laser pulse energy, number of overscans and geometrical pulse-to-pulse spacing are presented characterising the resulting surface structures qualitatively. Then, the periodicity for repeated structures is analysed using the fast Fourier transform (FFT) algorithm quantitatively (Mezera and Römer, 2019b). Finally, first results from adhesion tests of polyetherketoneketone (PEKK) polymer are presented.

2. Experimental

The investigated sample material consisted of AISI430 stainless steel which was mirror-polished to obtain an surface roughness of R_a < 15 nm. Prior to laser processing, samples were cleaned with ethanol-drenched swabs. A pulsed laser source (TruMicro5050, Trumpf GmbH & Co. KG, Germany) with pulse duration of 7 ps, a wavelength of 515 nm and a maximum repetition rate of 400 kHz as shown in figure 1(a) was used for the machining experiments. For beam manipulation, a galvanometric scanner system (IntelliScan 14, Scanlab GmbH, Germany) and an f-Theta lens with focal length of 100 mm was used achieving a focal beam radius ($d/2$) of 12.5 µm and spot positioning accuracy of about ±1 µm. The spatial beam profile was Gaussian with a M^2 value of <1.3. Samples were then analysed with a scanning electron microscope (SEM), as well as with a confocal scanning laser microscope (CSLM) for imaging and profile measurements respectively.

For adhesion tests, thin polymer films of PEKK were sandwiched between a machined and a pristine sample and heated in a furnace to a temperature of 385°C, above the polymer melting point and subsequently cooled at a rate of about < 1°C/min. Then, samples were separated and the machined sides were analysed with optical microscopy (VHX-5000, Keyence, Japan).

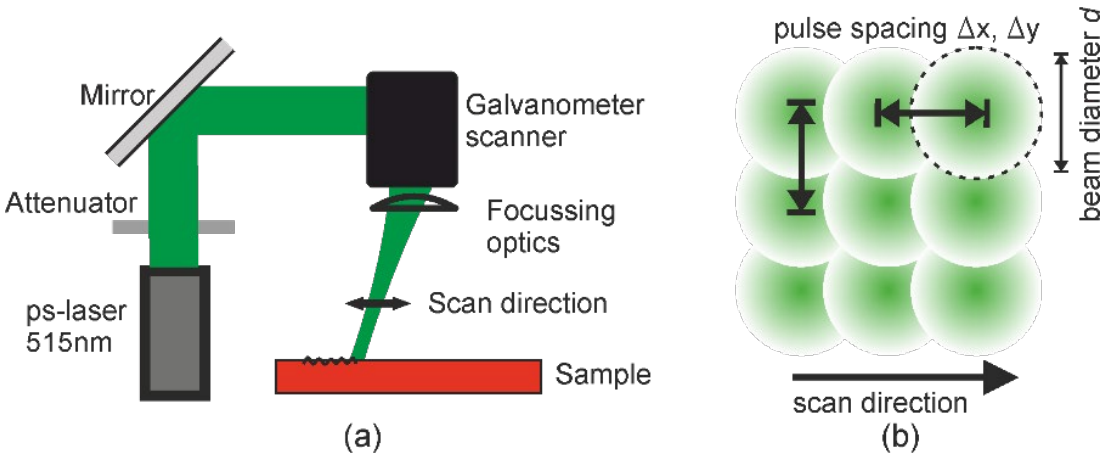

Fig. 1. (a) Schematic of laser setup; (b) Top view of single laser pulse distribution with definitions for parametric study.

3. Results

3.1. Parameter study

In this section, results of a parametric study on the samples are shown. The laser parameters of pulse energy E_p, number of overscans N_{OS} and geometrical pulse spacing $\Delta x,y$ ($\Delta x,y=\Delta x=\Delta y$) are varied in a range of $0.8 \cdot 10^{-7}$ - $6 \cdot 10^{-7}$ J, 1 - 50 and 2 - 40 µm respectively. The temporal pulse-to-pulse spacing was 100 µs corresponding to a repetition rate of 10 kHz. A schematic of the geometrical parameters is shown in figure 1(b).

3.2. Surface morphologies

For non-overlapping laser pulses ($\Delta x,y$ = 40 µm), the material removal rate per pulse as the maximum crater depth per pulse and per unit fluence was determined to be $(2.3 \pm 0.8) \cdot 10^{-6}$ µm·m^{-2}/J measured via CLSM. For instance, a single pulse with an energy of 5 µJ would ablate a crater with a depth of about 47 nm.

In the observed range of laser parameters, periodic structures formed rather readily above a specific damage threshold for which surface modifications were visually observed, and typical examples of low spatial frequency LIPSS (LSFL) (a), high spatial frequency LIPSS (HSFL) (b) and hierarchical structures (c) can be seen in figure 2. The orientation of these structures is approximately perpendicular to the linearly polarised beam for LSFL and shifted by 90° for HSFL, which is typical for LIPSS on metals (Al Bayaz et al., 2008; Nathala et al., 2015).

At fluence levels below the threshold at which LIPSS form, surface damage, e.g. seen in figure 3(a) was found on the sample, consisting of melting or delamination of pre-existing imperfections of the steel surface. For modifications fabricated at relatively large E_p and N_{OS}, non-deterministic hierarchical structures were also found, as shown in figure 3(b). There, some areas were ablated with a lower removal rate than their surroundings leading to mound-like structures, sometimes also referred to as pillars. Also, at relatively high number of overscans and high pulse energies, very fine nano-sized foam structures were found next to or on the modified surface (see figure 3(c)), likely originating from re-condensed matter and previously seen for ultrashort ablation (Grant-Jacob et al., 2019).

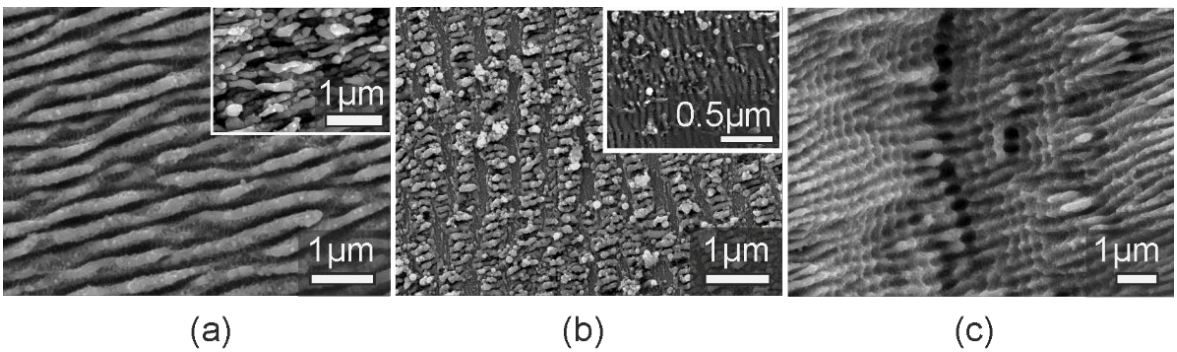

Fig. 2. SEM images of resulting types of laser-induced periodic surface structures (LIPSS) on stainless steel AISI430: (a) Low spatial frequency LIPSS (LSFL), (b) High spatial frequency LIPSS (HSFL) and (c) deterministic hierarchical structures with LSFL. Insets show respective LIPSS subtypes.

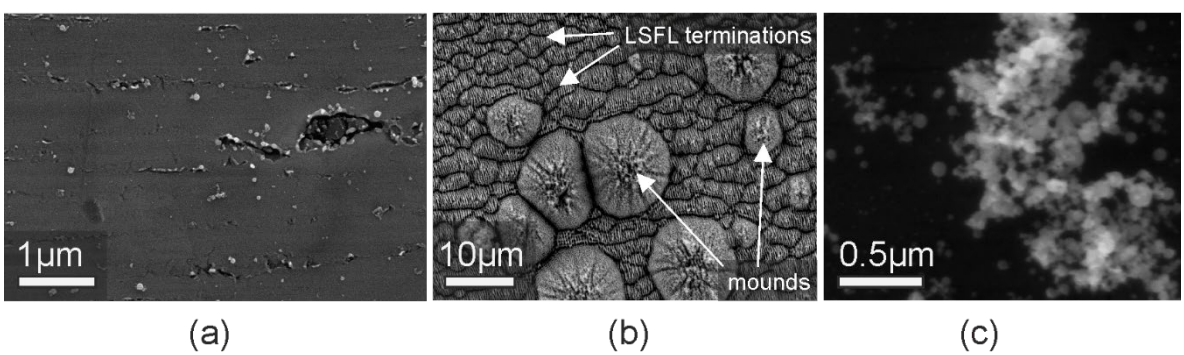

Fig. 3. SEM images of periodic and non-periodic features found on laser-machined stainless steel AISI430, such as (a) damage on surface imperfections, (b) non-deterministic hierarchical features with LIPSS regularly terminated by lines, and mounds ablated at a lower rate than surrounding areas; (c) Image of superficial nanoparticle (foam) aggregates.

The type of modifications were broadly categorised according to their periodicity (high and low spatial frequency LIPPS) and if ablation occurred (damage, hierarchical textures). For the highest fluence levels and pulse energies observed, ablation was always found in combination with LIPSS. In most cases where LSFL were observed, the space between single lamella or ripples appeared to contain HSFL. In the following characterisation however, only the most dominant structures are considered. Figure 4 shows the condition of the sample surface as a function of the maximum accumulated fluence F_a^{max} (or in the following also referred to as 'fluence'), pulse energy E_p and geometrical pulse-to-pulse spacing $\Delta x,y$. The maximum accumulated fluence and effective number of pulses per area N_{eff} was defined as (Mezera and Römer, 2019a):

$$F_a^{max} = N_{OS} F_0 \frac{\pi}{8(OL-1)^2}\left[1 + 2e^{-\left(\frac{\pi^2}{8(1-OL)^2}\right)}\right]^2 \quad (1)$$

$$F_0 = \frac{8E_p}{\pi d^2} \quad (2)$$

$$OL = 1 - \frac{\Delta x,y}{d} \quad (3)$$

$$N_{eff} = N_{OS}\frac{\pi}{8}\frac{d^2}{\Delta x \Delta y} = N_{OS}\frac{\pi}{8(OL-1)^2} \quad (4)$$

with E_p the pulse energy, *OL* the overlap ratio of consecutive beams (1 being complete overlap and 0 for two beams spaced apart further than the beam diameter *d*) and N_{OS} is the number of overscans.

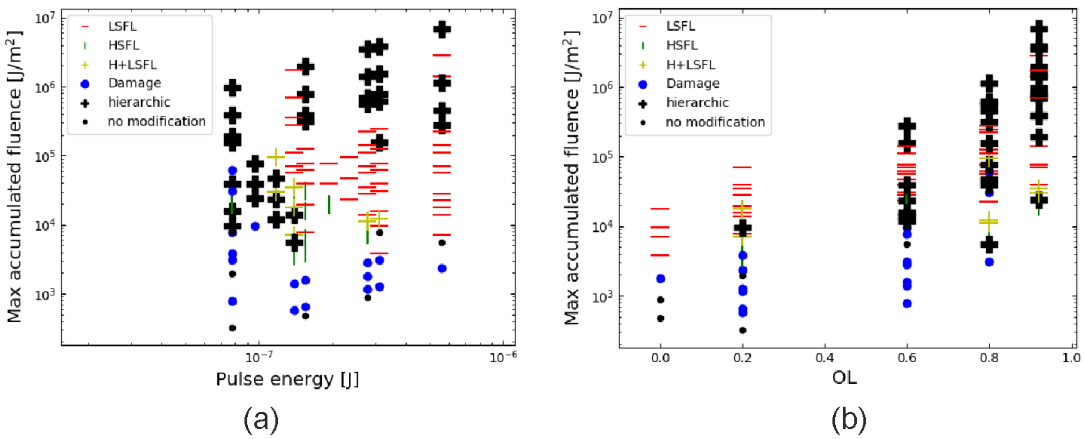

Fig. 4. Occurrence of surface features as (a) function of pulse energy and maximum accumulated fluence, and (b) geometrical overlap and maximum accumulated fluence.

As can be concluded from figure 4, the accumulated fluence level, in conjunction with the pulse energy, can explain the occurrence of LSFL which appear above a certain threshold ($F_a^{max} > 3{\cdot}10^3$ J/m^2, $E_p > 10^{-7}$ J) as a function of both parameters. Similarly, HSFL appear only in a limited range of fluence levels ($F_a^{max} = 3{\cdot}10^3$ - $4{\cdot}10^4$ J/m^2), and their appearance seems to depend also on other factors as seen in the overlap with different structures (damage, LSFL, etc.) as shown in figure 4(a). However, when studying the influence of pulse-to-pulse overlap (related to spacing via equation 3) and fluence as shown in figure 4(b), no clear distinction of structure is obtained, meaning that overlap does not uniquely determine the appearance of one or the other type of LIPSS.

3.3. Periodicity of LIPSS

For further quantitative characterisation, the periodicity of the surface features was retrieved via the FFT algorithm analysis (verified by manual measurements) of the SEM images for a subset of pulse energies (approx. $1{\cdot}10^{-7}$ - $3{\cdot}10^{-7}$ J) used in the previous section. Periodicities Λ were found in the range of 59.2 ± 11 nm and 379 ± 57 nm for HSFL and LSFL respectively. The distribution of periodicities is shown in figure 5(a) for different types of LIPSS and as a function of accumulated maximum fluence levels. The LSFL were subcategorised as standard LSFL (figure 2(a)), *terminated* LSFL (see figure 3(b)) and *dense* LSFL (figure 2(a), inset). HSFL were considered as a single type due to the limited range of conditions for which these structures emerged. While HSFL and LSFL are separated in figure 5(a) per definition, the subcategorization of LSFL can be seen in either the periodicity (dense LSFL) or fluence (standard versus terminated types). Also,

for the investigated set of pulse energies, HSFL form up to an accumulated fluence of approximately $2 \cdot 10^4$ J/m^2, while LSFL are mainly found above this value.

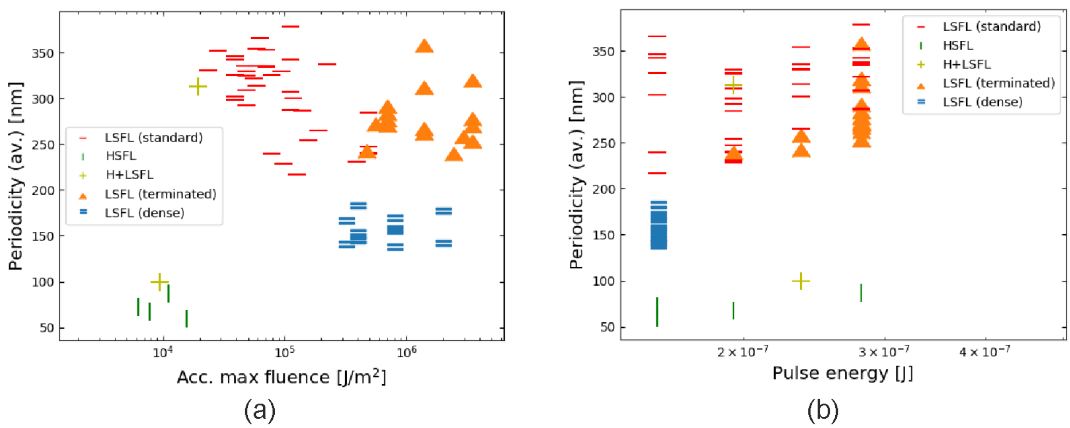

Fig. 5. Periodicity of LIPSS as a function of (a) accumulated fluence and (b) pulse energy.

However, no clear trend of periodicity as a function of the investigated laser parameters (e.g. pulse energy or spacing) could be concluded. Nonetheless, figure 5(a) suggests that at least for LSFL, a slight decrease in minimum periodicity as a function of fluence can be seen (Yasumaru et al., 2005).

There was no correlation found between periodicity of type as a function of pulse energy (figure 5(b)) or spacing (not shown). The effective number of pulses- of which maximum accumulated fluence F_a^{max} is a function- showed a similar trend as presented in figure 5(a) identifying HSFL for $N_{\text{eff}} \leq 25$ and LSFL for $N_{\text{eff}} \geq 25$. Thus, the latter parameters could predict the appearance of high or low periodicities of LIPSS.

3.4. Polymer adhesion tests

For initial testing of the influence of micro- and nanostructures on the mould surface on the adhesion of thermoplastic polymers to steel, PEKK films were molten in a sandwich of steel sample plates of which one underwent laser surface machining at different selected conditions, see figure 6(a). Areas with LSFL, HSFL and with micro craters (or dimples as hierarchical structures) were compared via heating of the PEKK films emulating the thermoplastic composites consolidation process. Here for simplicity we only applied comparable temperatures, but not the pressures of the real consolidation process. The latter would amount to a few bars and will further influence adhesion of the polymer on the steel sample. The resulting samples are shown in figure 6(b). Initial tests show that polymers were not homogeneously distributed over the sample mould areas, but formed droplets which covered the pristine steel surface (figure 6(b)-iii) as well as machined areas (figure 6(b)-i) and -ii)). The solidified polymer layer (fig.6(b)-iv) ruptured along its bulk (and not at the mould interface) and it was not clear if polymer would have partly been removed from mould areas.

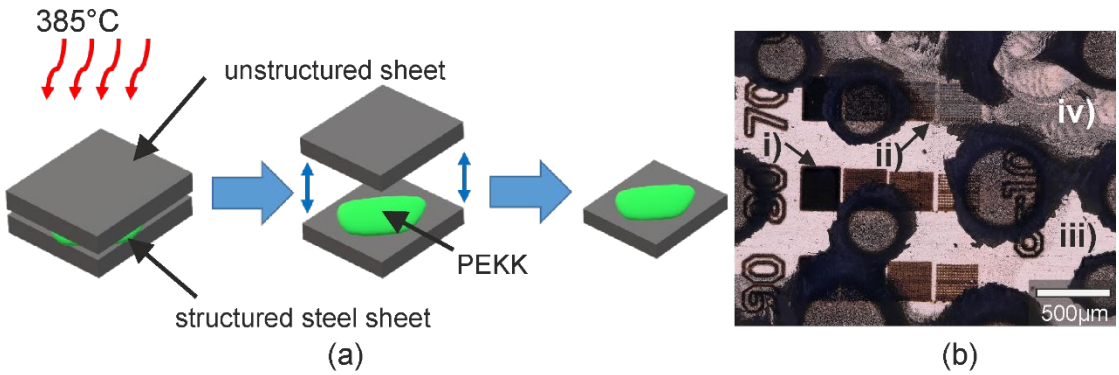

Fig. 6. (a) Schematic of adhesion experiment of PEKK films on machined steel sample; (b) Microscope image of laser-machined sample surface (i) partially covered with polymer (iv) after sandwich separation. The bare metal surface and the polymer are shown in (iii) and (iv) respectively.

Further studies need to be conducted with modified samples in which the presence of non-structured areas is reduced or treated with conventional release agent to reduce their influence on adhesion. Also the strength of the bulk of the polymers needs to be increased via introducing thermoplastic composites tapes instead of the polymer matrix alone.

4. Conclusions

For the surface texturing of a mould material for thermoplastic composites, a parametric study revealed regimes for creating surface structures on a micro- and nanoscale. Laser-induced periodic surface structures with periodicities Λ in the range of just below the wavelength λ (Λ=379 nm) down to $\lambda/9$ (Λ=59 nm) were found as a function of accumulated fluence, pulse spacing and effective number of pulses.

Macroscopic features were created with ablation rates of $(2.3 \pm 0.8)\cdot 10^{-6}$ µm·m^{-2}/J. Initial polymer adhesion tests with PEKK need to be followed-up by further experiments that will evaluate adhesion strength and visualise the crystalline structure of potential residues on laser-structured surfaces. Further studies aim at extending tests to nylon and other relevant polymers for composites with automotive and aerospace applications, and extend the range of laser-induced surface textures.

Acknowledgements

The authors would like to acknowledge funding from the program ‘Top Technology Twente: Connecting Industry’. We would like to thank Liangyong Chu, Wouter Grouve, Luigi Capuano, Ton Bor and Matthijn de Rooij for their input through scientific discussions and technical assistance.

References

Al Bayaz, A., Giani, A., Foucaran, A., Pascal-Delannoy, E., Boyer, A., Alti, K., … Liu, J., 2008. Metglas thin film based magnetostrictive transducers for use in long period fibre grating sensors, Journal of Applied Physics 18, 127–136.

Baudach, S., Bonse, J., Kautek, W., 1999. Ablation experiments on polyimide with femtosecond laser pulses, Applied Physics A: Materials Science & Processing 69, S395–S398.

Birnbaum, M., 1965. Semiconductor Surface Damage Produced by Ruby Lasers, Journal of Applied Physics 36, 3688–3689.

Bonse, J., Hohm, S., Kirner, S. V., Rosenfeld, A., Kruger, J., 2017. Laser-Induced Periodic Surface Structures— A Scientific Evergreen, IEEE Journal of Selected Topics in Quantum Electronics 23.

Critchlow, G. W., Litchfield, R. E., Sutherland, I., Grandy, D. B., Wilson, S., 2006. A review and comparative study of release coatings for optimised abhesion in resin transfer moulding applications, International Journal of Adhesion and Adhesives 26, 577–599.

Csete, M., Hild, S., Plettl, A., Ziemann, P., Bor, Z., Marti, O., 2004. The role of original surface roughness in laser-induced periodic surface structure formation process on poly-carbonate films, Thin Solid Films 453–454, 114–120.

Fauchet, P. M., Siegman, A. E., 1982. Surface ripples on silicon and gallium arsenide under picosecond laser illumination, Applied Physics Letters 40, 824–826.

Grant-Jacob, J. A., Mackay, B. S., Baker, J. A. G., Xie, Y., McDonnell, M. D. T., Health, D. J., … Mills, B., 2019. Patterned Nanofoam Fabrication from a Variety of Materials via Femtosecond Laser Pulses, Materials Sciences and Applications 10, 186–196.

Jee, Y., Becker, M. F., Walser, R. M., 1988. Laser-induced damage on single-crystal metal surfaces, Journal of the Optical Society of America B 5, 648.

Mezera, M., Römer, G. R. B. E., 2019a. Model based optimization of process parameters to produce large homogeneous areas of laser-induced periodic surface structures, Optics Express 27, 6012.

Mezera, M., Römer, G. R. B. E., 2019b. "Upscaling laser-induced periodic surface structures (LIPSS) manufacturing by defocused laser processing," In U. Klotzbach, R. Kling, & A. Watanabe (Eds.), Laser-based Micro- and Nanoprocessing XIII (p. 29). SPIE.

Nathala, C. S. R., Ajami, A., Ionin, A. A., Kudryashov, S. I., Makarov, S. V, Ganz, T., … Husinsky, W., 2015. Experimental study of fs-laser induced sub-100-nm periodic surface structures on titanium, Optics Express 23, 5915.

Packham, D. E., 2002. Mould Sticking, Fouling and Cleaning, RAPRA Report 13, 150.

Römer, G. R. B. E., Huis in't Veld, A. J., Meijer, J., Groenendijk, M. N. W., 2009. On the formation of laser induced self-organizing nanostructures, CIRP Annals 58, 201–204.

Römer, G. R. B. E., Skolski, J. Z. P., Oboňa, J. V., Ocelík, V., de Hosson, J. T. M., Huis in 't Veld, A. J., 2014. "Laser-induced periodic surface structures, modeling, experiments, and applications," In U. Klotzbach, K. Washio, & C. B. Arnold (Eds.), Proceedings Volume 8968, Laser-based Micro- and Nanoprocessing VIII (p. 89680D). SPIE.

Siegrist, M., Kaech, G., Kneubühl, F. K., 1973. Formation of a periodic wave structure on the dry surface of a solid by TEA-CO2-laser pulses, Applied Physics 2, 45–46.

Temple, P., Soileau, M., 1981. Polarization charge model for laser-induced ripple patterns in dielectric materials, IEEE Journal of Quantum Electronics 17, 2067–2072.

Yasumaru, N., Miyazaki, K., Kiuchi, J., 2005. Fluence dependence of femtosecond-laser-induced nanostructure formed on TiN and CrN, Applied Physics A: Materials Science and Processing 81, 933–937.

Young, J. F., Preston, J. S., van Driel, H. M., Sipe, J. E., 1983. Laser-induced periodic surface structure. II. Experiments on Ge, Si, Al, and brass, Physical Review B 27, 1155–1172.